DOI: 10.1002/cphc.200((will be filled in by the editorial staff))

Higher gas solubility in nano-liquids?

Sylvain Miachon*[a], Victor V. Syakaev[a], Aydar Rakhmatullin[a], Marc Pera-Titus[a], Stefano Caldarelli[b] and Jean-Alain Dalmon[a]

The influence of a system scale on its physicochemical properties is still a matter of discussion. Particularly, in nanometre-confining porous media, the structure[1,2], dynamics[1,3-7] and physical behaviour[8-16] of condensed matter differ from what is observed at the macroscopic level. Nevertheless, little work is available for 3-phase systems at a nano-scale[8,17,18]. Many natural and technological processes hinge on a solid-gas-liquid contact in a confined environment, for instance in porous nanometric cavities. Relevant examples may be as diverse as some geological phenomena, such as oil natural formation, gas and petroleum extraction and storage, chromatographic analysis, some membrane-based processes or heterogeneous catalytic reactions[18-21]. Herein we provide experimental evidence of a dramatic increase of hydrogen and light hydrocarbon solubility in solvents confined in mesoporous solids.

The solubility of a gas in a bulk solvent is conventionally described by Henry's Law, which establishes a linear relationship between the concentration of a dissolved gas and its partial pressure above the solvent. Despite the general acceptance of this equation, some previous kinetic studies carried out in gas-liquid catalytic membrane reactors for nitrobenzene hydrogenation[22] have suggested that it might be limited when the solvent is confined in a mesoporous matrix. Contrary to what would be expected, a zero-order kinetics is observed for the gas reactant when molecular hydrogen and liquid nitrobenzene are put into contact using a catalytic membrane contactor. This experimental observation might be interpreted in terms of an *oversolubility* of molecular hydrogen in the liquid nano-volume confined inside the pores, where the catalysis might benefit from a higher hydrogen concentration. Recently, this type of effect has been predicted by Molecular Dynamics for molecular nitrogen and oxygen in nano-confined water[17].

Despite the small range of signal position variations for the molecules studied here (e.g. compared to ^{129}Xe[23]) when exposed to a mesoporous solid partially filled with an aprotic solvent, we were able to characterize and unambiguously assign seven ^{1}H-NMR signals for all the tested gases as a function of the local environment (see Exp. Section).

Table 1. Values of H_2, CH_4 & C_2H_6 solubility (ℓ_α [%]), in CCl_4 and CS_2 in different environments using γ-Al_2O_3 (*) and silica (**) as confining agents. The gas pressure was kept at 100-120 kPa in all experiments.

System at equilibrium with gas phase:	CCl_4			CS_2	
	H_2	CH_4	C_2H_6	H_2	CH_4
1. Bulk solvent	8.5 ± 1 (8.6)	67 ± 7 (73)	578 ± 6 (554)	5 ± 1 (6.6)	56 ± 6 (52)
2. Bulk solvent with porous solid	8.5 ± 1*	66 ± 7* 71 ± 7**	453 ± 50*	5 ± 1*	56 ± 16* 50 ± 10**
3. Solvent confined in mesopores	34 ± 6*[d]	169 ± 4*[a] 144**[c]	1057 ± 114*[a]	24 ± 1*[d]	252*[a] 125**[b]

[a] Values in parentheses refer to literature[24]. Row 3, values obtained for mean confined system sizes $\bar{d}$ [nm]: [a]3.0-3.7, [b]7.8, [c]6.8, [d]8.3-9.2.

Although γ-alumina and silica show a weak H_2 and light hydrocarbon adsorption behaviour at ambient conditions (molar loadings of 0.002, 0.09 and 1.0 $mmol \cdot g^{-1}$ for H_2, CH_4 and C_2H_6 in γ-alumina, respectively, have been experimentally determined by micro-volumetry), in all cases no signal related to gas interaction with neither adsorbed thin-film-liquid nor co-adsorption on the pore walls was detected. Moreover, in the case of ethane, its extremely low surface tension values prevent it from undergoing capillary condensation in open mesopores under the pressures used in this work (<500 kPa)[25].

The concentration of a target molecule in each phase was measured against an external standard that can be well-resolved in the NMR spectra. The solubility values obtained for all the tested gases in different liquid-solid configurations are summarized in Table 1. As it can be seen, our method reproduces fairly well experimental gas solubility data in bulk CCl_4 and CS_2 (case 1). Case 2 describes an experiment where the gas molecules are dissolved in the bulk solvent containing the porous solid. In this case, two peaks can be observed, corresponding to rows 5 and 6 in Table 2 (respectively H_2 in the bulk and in the pores). Both peak integrations match the bulk solubility values. On the opposite, case 3 shows a single peak providing gas solubilities enhanced by a factor 2 to 5 over the corresponding bulk values for all gases when the solvent is confined in the solid mesopores, namely for solvent loadings lower than the total pore volume of the solids. This observation suggests a role of meso-confined gas-liquid interfaces in enhancing gas solubility.

To gain more insight into this hypothesis, a number of experiments were performed where the gas solubility was measured for decreasing meso-confined liquid sizes. This could be accomplished in practice by reducing the solvent loading in the porous volume of the target solid. The nano-liquid mean size, $\bar{d}$,

[a] *Dr. S. Miachon, Dr. V. V. Syakaev, Dr. A. Rakhmatullin, Dr. M. Pera-Titus, Prof. J.A. Dalmon*
Institut de Recherches sur la Catalyse et l'Environnement de Lyon (IRCELYON), UMR5256 CNRS / Université Claude Bernard Lyon 1
2 avenue A. Einstein, 69626-Villeurbanne Cedex (France)
Fax: +33 (0) 472445399
E-mail: sylvain.miachon@ircelyon.univ-lyon1.fr

[b] *Prof. S. Caldarelli*
JE 2421 TRACES (Université de Provence et Paul Cézanne)
Site de Saint Jérôme, Service 511, 13013-Marseille (France)

Supporting information for this article is available on the WWW under http://www.chemphyschem.org or from the author.

corresponding to a particular solvent loading, *f*, could be measured and tuned from the cumulative pore volume distribution (Broekhoff-de-Boer, BDB, from N_2 desorption at 77 K) of the target solid by Eq. 1 (see SI-b for more details)

$$\bar{d} = \left[\frac{1}{V(f)} \int_0^{V(f)} (d - 2t)^3 \, \delta V \right]^{1/3} \qquad (1)$$

where it has been implicitly assumed that the mesopores are slit-shaped. In our calculations, the statistical thickness of the adsorbed CCl_4 and CS_2 layer, 2*t*, was computed using the expressions provided by Hakunan and Naono[26] from their studies on MCM-type mesoporous silica solids (pore size ranging from 2.0 to 10 nm) in the P/P_0 range 0.08-0.60.

According to the BET classification, the adsorption of CCl_4 on mesoporous adsorbents with mean pore sizes lying in the range 2-110 nm and for temperatures in the range 283.15-308.15 K follows a Type V isotherm[26], which involves Kelvin-type capillary condensation of the vapour before formation of an adsorbed monolayer on the porous surface, together with no remarkable hysteresis between adsorption and desorption curves for mean pore sizes <10 nm. Note that this isotherm differs from that obtained for N_2 adsorption at 77 K (type IV), where vapor condensation appears after the formation of an adsorbed multilayer on the porous surface. Therefore, in a typical experiment carried out in this study, CCl_4 desorption at room temperature proceeds from larger to smaller pores, keeping an adsorbed monolayer of 0.38-0.65 nm in thickness on the evacuated pores at P/P^0>0.40 for both solids that prevents the target gas from adsorbing on the evacuated pore walls. This picture is consistent with the experimental fact that no RMN signal corresponding to adsorbed species is observed for all the tested conditions. In this study, only experiments involving adsorbed solvent accounting for a volume <15% of the liquid loading have been considered (P/P^0 > 0.50 and >0.70 for γ-alumina and silica, respectively, see SI-e,f).

Figure 1 shows the effect of tuning the meso-confined mean size on gas solubility. As can be seen, gas solubility appears to be strongly enhanced for nano-liquid sizes lower than 10 nm, as long as gas-liquid interfaces are confined in the mesoporous system, while the bulk values tend to be recovered when the solid is completely soaked by the liquid. To evaluate in more detail the role of meso-confined gas-liquid interfaces in enhancing gas solubility, an additional experiment was performed where methane was dissolved in a thin and extended CCl_4 layer on a 7-$m^2 \cdot g^{-1}$ macroporous γ-alumina sample (ca. 15 nm thickness or ~30 molecular layers, based on weight uptake and the specific surface area of the solid probe). Our results reveal a methane solubility enhancement up to 230%, thus confirming the contribution of gas-liquid interfaces in the observed phenomenon.

Gas-liquid interfaces are usually described from computer modeling, as dense gas-like regions of several molecular diameters in thickness[27,28]. The concentration of H_2, CH_4 and C_2H_6 adsorbed at a gas-liquid interface, or simply surface excess, $\Gamma_g^{(1)}$, follows a type I behavior according to the Gibbs classification, which is much higher than that in each section of a bulk liquid far from the surface. Moreover, higher values might be also expected from surface tension reduction due to curvature in mesopores[29]. As this interface accounts for a significant part of the volume in liquid-filled mesopores, the apparent *oversolubility* might be at least partially attributed to meso-confined interfacial liquid layers.

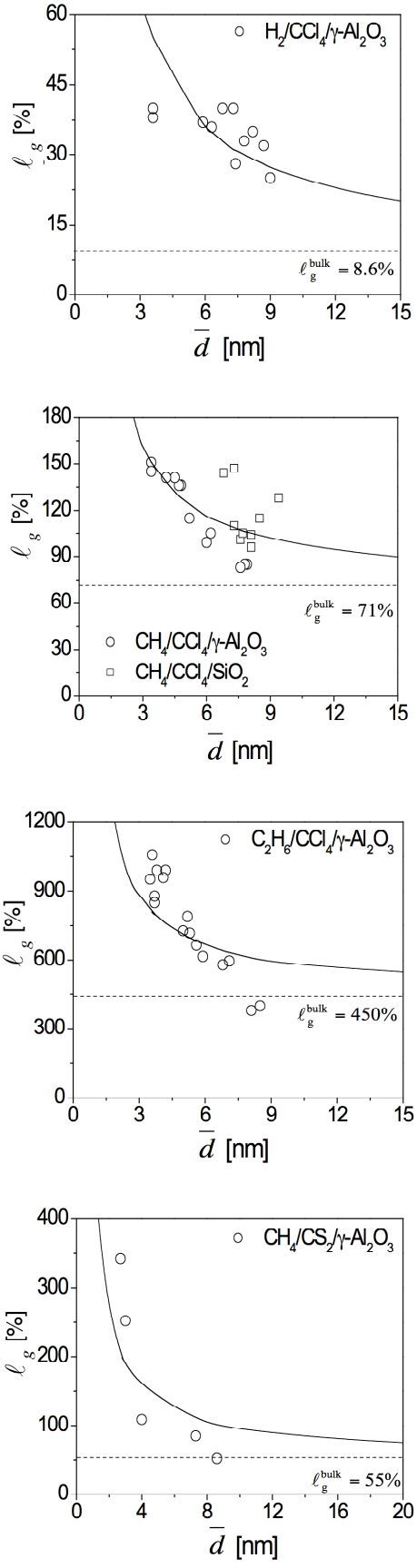

Figure 1. Evolution of H_2, CH_4 and C_2H_6 solubility in CCl_4 confined in mesoporous γ-alumina and silica with the nano-liquid mean size. The solid and dashed lines refer, respectively, to the trends predicted by Eq. 2 and to the bulk solubility values.

This idea can be reinforced using a mass balance-based model relying on the general picture of a filled mesopore illustrated in Figure 2. Regarding a gas-liquid interface confined in a mesopore, assuming that its thickness, *z*, is constant and approaching the molecular size of the target gas (2.9, 3.5 and 3.8 Å for H_2, CH_4 and C_2H_6, respectively), see SI-g for further details, the overall gas solubility, ℓ_g, can be accounted for by Eq. 2

$$\ell_g = \ell_g^{bulk} + \frac{1}{d}\left(\frac{\Gamma_g^{(1)}}{C_G} - z\,\ell_g^{bulk}\right) \qquad (2)$$

where ℓ_g^{bulk} is the bulk solubility. As shown in Figure 1, the trends predicted by Eq. 2 are close to those observed for H_2, CH_4 and C_2H_6 in CCl_4 and CS_2 confined in γ-alumina and silica as a function of the nano-liquid mean size. The model predicts recovery of bulk solubility for nano-liquid sizes beyond 15-20 nm.

Furthermore, the surface excesses predicted for H_2, CH_4 and C_2H_6 in CCl_4 confined in γ-alumina and silica are, respectively, 0.04, 0.07 and 0.35 molecules·nm^{-2}, while that predicted for CH_4 in CS_2 confined in γ-alumina is 0.10 molecules·nm^{-2}. These values compare well with those obtained for adsorption of each gas at the surface of bulk liquids (e.g., water), as measured from the variation of surface tension with hydrostatic pressure using the Gibbs equation (0.01, 0.04 and 0.12 molecules·nm^{-2}, respectively, for H_2, CH_4 and C_2H_6)[30]. Note that in all cases, the surface excesses found in the present study are much lower than 5 molecules·nm^{-2} corresponding to a complete adsorbed monolayer on the liquid surface.[30]

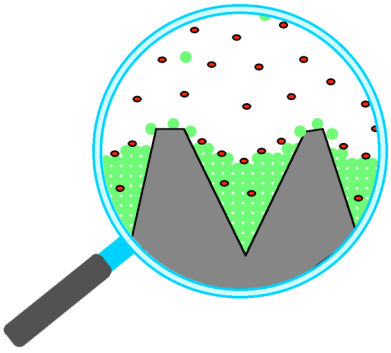

Figure 2. Pictorial representation of gas solubility enhancement due to solvent nano-size. The gas molecules (CH_4 in this case) are drawn in red, the solvent molecules (CCl_4) in green and the confining solid in grey. This expanded view shows, at a realistic scale, the approximate amount of gas molecules in different states for a mean pore size of about 6 nm.

Finally, on the basis of the observed solubility enhancement in nano-liquids, the selection of a solvent with higher affinity to H_2 could be foreseen as a strategy for its storage. For instance, using hexane confined in low-density mesoporous materials (e.g., silica aerosol), a stored quantity up to 6 g H_2 / kg wet solid can be computed at 298 K and 5000 kPa. In this estimate, an *oversolubility* factor of 4 has been taken into account according to Table 2, and the gas solubility has been assumed to evolve linearly with pressure. Moreover, optimizing the proportion of liquid in the interfacial state by tailoring the pore geometry, higher stored values can be imagined. For comparison, under similar storing conditions, the best reference storage materials (i.e. metallic hydrides) would store up to 20 g H_2/kg[31] Furthermore, gas solubilization in nano-solvents might offer the added advantage of fast reversibility due to the high gas-liquid contact surface area. Hence, H_2 could be either stored or released by simply quenching or heating.

In conclusion, we provided experimental evidence that reducing solvent volume down to nanometre scales, by means of confinement in mesoporous materials, induces a dramatic increase of gas solubility. If the sample is regarded as a whole, the bulk Henry's solubility constant no longer applies at these conditions. The expression of the solubility has been therefore modified to take into account the quantitative contribution of the gas-liquid interface at this scale. Surface excess values were found to be in good keeping with previous macroscopic measurements. On the basis of the observations reported here, the *oversolubility* effect seems to be a general one, which deserves further attention for possible applications in gas storage and separation, as well as potential implications in reactor engineering.

Experimental Section

There are very few studies in the literature dealing with the measurement of gas solubilities in liquids in restricted geometries.[18] Therefore, we devised a specific protocol to measure hydrogen and light hydrocarbon (methane and ethane) solubilities by proton Nuclear Magnetic Resonance (^{1}H-NMR). Briefly, the measurements were performed using a NMR tube equipped with a Young valve for gas tightness. The confining solids were mesoporous γ-alumina GFS400 (235 m^2 g^{-1}) and silica 432 (309 m^2 g^{-1}) and macroporous alumina SPH512 (7 m^2 g^{-1}), all supplied by Rhône-Poulenc. The resulting Carbon tetrachloride (CCl_4) and carbon disulfide (CS_2), 99.99% purity, both from Fluka, were selected as aprotic solvents to avoid any interference in the ^{1}H-NMR analyses. All sample handling was carried out under dry nitrogen atmosphere.

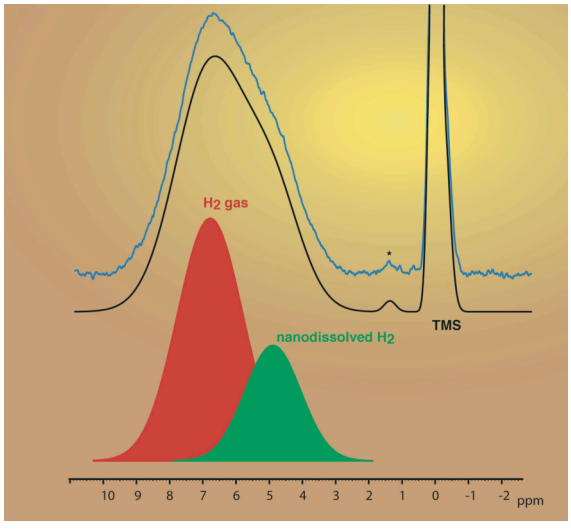

Figure 3. ^{1}H-NMR spectrum of a sample featuring H_2 nano-dissolved in CCl_4 confined in porous γ-Al_2O_3. The solvent is present only inside Al_2O_3 pores. The peak at 0 ppm is from a sealed reference capillary containing a solution of TMS in CCl_4. The symbol (*) corresponds to residual traces of H_2O. From top to bottom: experimental spectrum, calculated spectrum, relevant components as calculated (H_2 gas at about 6.7 ppm and H_2 dissolved in confined CCl_4 at 5.0 ppm, rows 3 and 7 in Table 1).

The porous solid, outgassed and dried overnight at 823 K under vacuum, was transferred to the NMR tube. It was then soaked with a large volume of solvent that was *in situ* degassed and evaporated down to the desired loading, as monitored by weight change. The target gas (H_2, CH_4 and C_2H_6, all 99.9999% purity, Air Liquide) was

fed into the tube at 100-120 kPa and room temperature (288-293 K). The whole system was then transferred to an NMR Bruker DSX spectrometer (300 MHz). The spectra were recorded with a spin echo pulse sequence and a spectral width of 18 kHz (32 and 256 scans acquired, respectively, in the absence and presence of the porous solid). The recycling and echo delays were kept at 10 s and 15 µs, respectively. Chemical shifts are given in parts per million (δ / ppm) relative to TMS.

A typical ^{1}H-NMR spectrum of H_2 when the solvent is only present inside the mesopores is plotted in Figure 3. A complete collection of spectra for H_2 in different environments are provided in SI-d. The different signals were identified by deconvolution of overlapping peaks in the spectra using Lorentzian curves and a linear baseline correction with WIN-NMR software, combined with variation of the packing/solvent loading conditions.. As an example, Table 2 summarizes the ^{1}H-NMR chemical shifts and signal widths obtained for molecular hydrogen: in the gas phase, either alone (row 1) or in contact with the dry (row 2) and wet (row 3) porous solid; dissolved in the bulk solvent alone (row 4) or containing the porous solid (row 5); dissolved in the meso-confined solvent either with (row 6) or without (row 7) solvent outside the pores. The assignment of signal 7 to nano-dissolved gas (row 7, Table 2) was confirmed by monitoring the temporal evolution of its intensity in a desorption experiment. The ^{1}H-NMR chemical shifts obtained for methane and ethane are listed in Table SI-1 (SI-c).

Table 2. ^{1}H-NMR signal position and peak width of H_2 in gas phase or dissolved in CCl_4 and CS_2 solvents in different environments. Chemical shifts (δ) are related to TMS as an external standard, without correction of diamagnetic susceptibility.

Signals for H2	δ [ppm]	Width [ppm]	Spectrum type (SI-d)
1. Gas alone	7.2 ± 0.2	2.1 ± 0.1	A
2. Gas in the presence of dry porous solid	6.0 ± 0.1	0.9 ± 0.4	B
3. Gas in the presence of wet porous solid	6.7 ± 0.2*	2.3 ± 0.4	E1 / E2
4. Dissolved in bulk solvent alone	4.65	0.01	C
5. Dissolved in bulk solvent in presence of porous solid	4.59 ± 0.07*	0.8 ± 0.5	D1 / D2
6. Dissolved in the solvent present in solid mesopores when the solid is soaked in bulk solvent	4.20 ± 0.01*	0.46 ± 0.05	D1 / D2
7. Dissolved in the solvent confined in solid mesopores when the gas/liquid interface is in the pore	5.0 ± 0.1*	1.9 ± 0.3	E1 / E2

* from deconvolution

Gas solubilities are given as the ratio of the gas dissolved in the solvent to that in the gas phase ($\ell_g = C_L / C_G$). In these calculations, the area of the NMR peaks, I_i, was assumed to be proportional to the number of protons, $n_{H,i}$, contributing to the signal i in the analyzed volume. Absolute concentrations were obtained with respect to a well-resolved external reference solution of TMS for H_2 and $CHCl_3$ for CH_4 and C_2H_6 in a sealed capillary (8% in volume in CCl_4 to produce peaks comparable to those of dissolved gas) inside the NMR tube. Dissolution equilibrium was reached after several minutes. The external solution was calibrated accurately at each measurement by comparison against a bulk solution of TMS ("100%" Euriso-Top, 0.75 mL) in $CDCl_3$ (0.03 v/v%). In all measurements, the NMR response was assumed to be the same for protons in the bulk and in the capillary. In these conditions, $C_{\ell,i}$ can be estimated by Eq. SI-1.

$$C_{\ell,i} = \frac{n_{H,R} C_R^o}{n_{H,R} f \varepsilon} \left(\frac{I_i^e}{I_{R,cap}^e} \right) \left(\frac{I_{R,cap}^o}{I_R^o} \right) \qquad (3)$$

where $n_{H,R}$ and $n_{H,i}$ are the number of protons, respectively, in the external reference solution and in the target gas i, C_R^0 is the concentration of the external reference in the calibration solution, I_i^e and $I^e_{R,cap}$ are, respectively, the peak areas of the target gas i and of the capillary reference obtained in an experiment, and $I^e_{R,cap}$ and I^e_R are the reference peak areas, respectively, in the capillary and in the calibration solutions. Finally, parameter ε is the fraction of the NMR tube volume filled up with solvent, which depends on the actual measurement. This parameter equals 1 in case of a bulk solvent, the solid intraporosity in case of a confined solvent (0.38 and 0.46 for γ-alumina and silica, respectively), or the sum of intraporosity and void fraction in the analyzed volume in case of a bulk solvent soaking the solid (0.84 and 0.82 for γ-alumina and silica, respectively).

Acknowledgements

This work was supported by the CNRS, the Rhône-Alpes Region and the French Ministry of Research.

Keywords: gas solubility · nano-liquid · Henry's law · hydrogen · light hydrocarbons

[1] V. Crupi, D. Majolino, P. Migiardo, V. Venuti, M. C. Belissent-Funel, *Molec. Phys.* **2003,** *101*, 3323-3333.
[2] P. Smirnov, T. Yamaguchi, S. Kittaka, S. Takahara, Y. Kuroda, *J. Phys. Chem. B.* **2000,** *104*, 5498-5504.
[3] C. Mattea, R. Kimmich, I. Ardelean, S. Wonorahardjo, G. Farrher, *J. Phys. Chem.* **2004,** *121*, 10648-10656.
[4] J. Baugh, A. Kleinhammes, D. Han, Q. Wang, Y. Wu, *Science.* **2001,** *294*, 1505-1507.
[5] Y. Ryabov, A. Gutina, V. Arkhipov, Y. Feldman, *J. Phys. Chem. B.* **2001,** *105*, 1845-1850.
[6] J. P. Korb, L. Malier, F. Cros, S. Xu, J. Jonas, *Phys. Rev. Lett.* **1996,** *77*, 2312-2315.
[7] P. E. Sokol, M. R. Gibbs, W. G. Stirling, R. T. Azuah, M. A. Adams, *Nature.* **1996,** *379*, 616-618.
[8] L. D. Gelb, K. E. Gubbins, R. Radhakrishnan, M. Sliwinska-Bartkowiak, *Rep. Prog. Phys.* **1999,** *62*, 1573-1659.
[9] H. K. Christenson, *J. Phys. Condens. Matter.* **2001,** *13*, R95-R113.
[10] J. Czwartos, B. Coasne, K. E. Gubbins, F. R. Hung, M. Sliwinska-Bartkowiak, *Molec. Phys.* **2005,** *103*, 3103-3113.
[11] R. J. Mashl, S. Joseph, N. R. Aluru, E. Jakobsson, *Nano. Lett.* **2003,** *3*, 589-592.
[12] J. K. Brennan, W. Dong, *J. Chem. Phys.* **2002,** *116*, 8948-8958.
[13] S. Senapati, A. Chandra, *J. Phys. Chem. B.* **2001,** *105*, 5106-5109.
[14] M. A. G. Zevenbergen, D. Krapf, M. R. Zuiddam, S. G. Lemay, *Nano. Lett.* **2007,** *7*, 384-388.
[15] F. Volino, H. Gérard, S. Miachon, *Ann. Phys.* **1997,** *22*, 43-82.
[16] E. Tombari, G. Salvetti, C. Ferrari, G. P. Johari, *J. Chem. Phys.* **2005,** *122*, 104712-104719.
[17] A. Luzar, D. Bratko, *J. Phys. Chem. B.* **2005,** *109*, 22545-22552.
[18] P. S. Rallabandi, D. M. Ford, *J. Membr. Sci.* **2000,** *171*, 239-252.
[19] A. A. C. M. Beenackers, in *Handbook of Heterogeneous Catalysis* (Eds: G. Ertl, H. Knözinger, J. Weitkamp), VCH, Weinheim, **1997**, pp. 1444-1464.
[20] Y. H. Guo, K. H. Langley, F. E. Karash, *Phys. Rev. B. Condens. Matter.* **1994,** *50*, 3400-3403.
[21] A. S. Kovvali, K. K. Sirkar, *Membr. Sci. Technol. Ser.* **2003,** *8*, 147-164.

[22] J. Peureux, M. Torres, H. Mozzanega, A. Giroir-Fendler, J. A. Dalmon, *Catal. Today*. **1995,** *25*, 409-415.
[23] C. I. Ratcliffe, *Ann. Rep. NMR. Spectr*. **1998,** *36*, 124.
[24] W. Gerrard, in *Gas solubilities: widespread applications*, Pergamon Press, Oxford**, 1980**, pp. 497.
[25] B. Liu, W. C. Wang, X. R. Zhang, New Author, *Phys. Chem. Chem. Phys.* **2004,** *6*, 3985-3990.
[26] M. Hakuman, H. Naono, *J. Colloid. Int. Sci*. **2001,** *241*, 127-141.
[27] A. Braslau, M. deutsch, P. S. Pershan, A. H. Weiss, *et al*., *Phys. Rev. Lett.* **1985,** *54*, 114-117.
[28] P. Davidovits, J. H. Hu, D. R. Worsnop, M. S. Zahniser, C. E. Kolb, *Farad. Disc*. **1995,** *100*, 65-82.
[29] D. S. Choi, M. S. Jhon, H. Eyring, *J. Chem. Phys*. **1970,** *53*, 2608-2614.
[30] R. Massoudi, A. D. King, *J. Phys. Chem*. **1974,** *78*, 2262-2266.
[31] A. Züttel, *Naturwissenschaften* **2004,** *V91*, 157-172.

Received: ((will be filled in by the editorial staff))
Published online: ((will be filled in by the editorial staff))

Entry for the Table of Contents (Please choose one layout)

Layout 1:

COMMUNICATIONS

Beyond Henry's law: When the system dimension is down to a few nanometers, gas solubility increases widely. H_2, CH_4 and C_2H_6 solubility values in two solvents where obtained by quantitative ^{1}H-NMR. A mass-balance model involving the gas-liquid interface zone is in good keeping with the observed variation. Application to H_2 storage is considered.

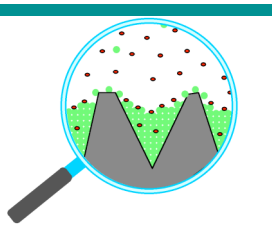

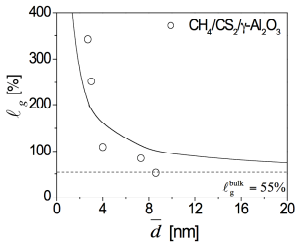

Sylvain Miachon, Victor V. Syakaev, Aydar Rakhmatullin, Marc Pera-Titus, Stefano Caldarelli and Jean-Alain Dalmon*

Page No. – Page No.

Higher gas solubility in nano-liquids?

Layout 2:

COMMUNICATIONS

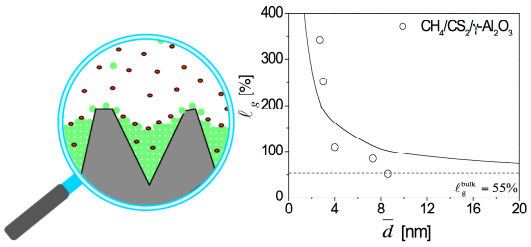

Beyond Henry's law: When the system dimension is down to a few nanometers, gas solubility increases widely. H_2, CH_4 and C_2H_6 solubility values in two solvents where obtained by quantitative ^{1}H-NMR. A mass-balance model involving the gas-liquid interface zone is in good keeping with the observed variation. Application to H_2 storage is considered.

Sylvain Miachon, Victor V. Syakaev, Aydar Rakhmatullin, Marc Pera-Titus, Stefano Caldarelli and Jean-Alain Dalmon*

Page No. – Page No.

Higher gas solubility in nano-liquids?

DOI: 10.1002/cphc.200((will be filled in by the editorial staff))

Higher gas solubility in nano-liquids?

Supporting information

Sylvain Miachon*[a], Victor V. Syakaev[a], Aydar Rakhmatullin[a], Marc Pera-Titus[a], Stefano Caldarelli[b] and Jean-Alain Dalmon[a]

SI-a: Determination of mesoconfined liquid sizes for a given solvent loading (physical meaning of Eq. 1)

Given a normal pore size distribution (as obtained for γ-alumina and silica for N_2 adsorption / desorption at 77 K), the mean liquid size related to a particular solvent loading, *f*, is computed as the mean pore size of the filled area, as shown in Figure A1. In the calculations using Eq. 1, the contribution of the statistical thickness of an adsorbed monolayer on the evacuated pores has also been taken into account.

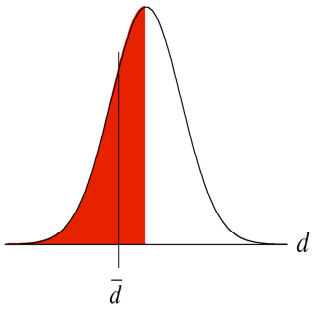

Figure A1

SI-b ^{1}H-NMR spectra of methane and ethane (Table SI-1)

Table SI-1. ^{1}H-NMR signal position and peak width for CH_4 and C_2H_6 in different environments for CCl_4 and CS_2 solvents using γ-Al_2O_3 as confining agent. Chemical shifts related to TMS as external standard, without correction of diamagnetic susceptibility. Values obtained for the confined liquid size in γ-Al_2O_3 [nm]: [a]2.5-6.1, [b]2.1-3.4, [c]2.1-5.8.

Signals	CH_4		C_2H_6	
	δ[ppm]	Width [ppm]	δ[ppm]	Width [ppm]
1. Gas alone	2.57 ± 0.03	0.01	3.22 ± 0.02	0.01
2. Gas in the presence of dry porous solid	1.6 ± 0.1*	0.96	2.29 ± 0.03*	0.8 ± 0.2
3. Gas in the presence of wet porous solid	1.5 ± 0.2*	1.3 ± 0.4	2.3 ± 0.2*	1.0 ± 0.3
5. Dissolved in bulk solvent alone	0.074	0.01	0.89	0.01
5. Dissolved in bulk solvent in presence of porous solid	-0.056*	0.46	0.93 / 0.53*	0.35 / 0.56
6. Dissolved in the solvent present in solid mesopores when the solid is soaked in bulk solvent	-0.4 ± 0.1*,a	1.4 ± 0.9	0.15 ± 0.07*,b	0.63
7. Dissolved in the solvent confined in solid mesopores when the gas/liquid interface is in the pore	0.69 ± 0.07*,a	1.3 ± 0.4	1.50 ± 0.08*,c	1.4 ± 0.3

* from deconvolution

SI-c NMR Spectra. This section shows ^{1}H-NMR of hydrogen in the different situation described in Table 2 in the paper.

A. H_2 gas alone (P = 110 kPa, T = 298 K)

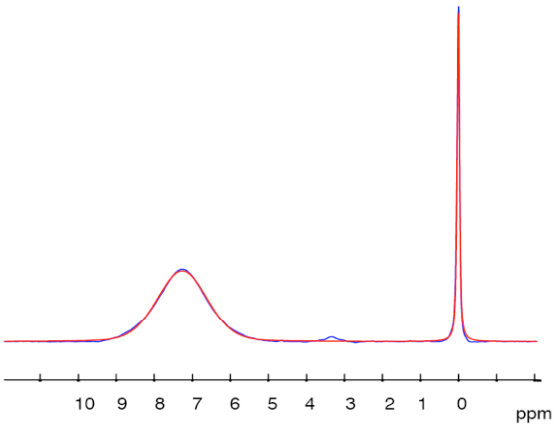

Number	δ [ppm]	Width [Hz]	I [-] (relative)	Correspondence in Table 2
1	7.26	885	1.00	row 1
2	-0.00	218	1.05	TMS
3	0.04	17	0.03	TMS

B. H_2 in contact with the dry porous solid (γ-alumina GFS400) (P = 110 kPa, T = 298 K)

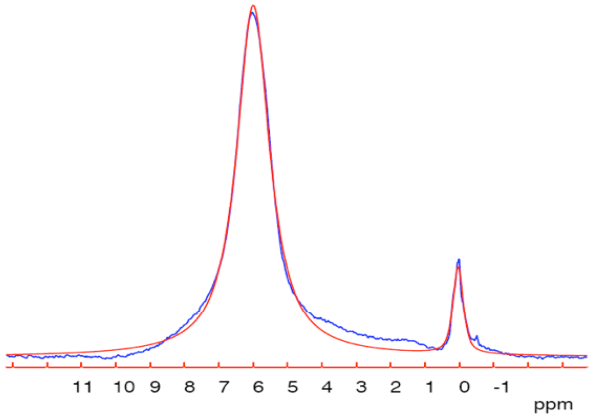

Number	δ [ppm]	Width [Hz]	I [-] (relative)	Correspondence in Table 2
1	6.02	350	1.00	row 2
2	3.56	660	0.06	water
3	1.52	282	0.02	TMS
4	0.03	105	0.07	TMS

C. H_2 dissolved in the bulk solvent alone (CCl_4) (P = 110 kPa, T = 298 K)

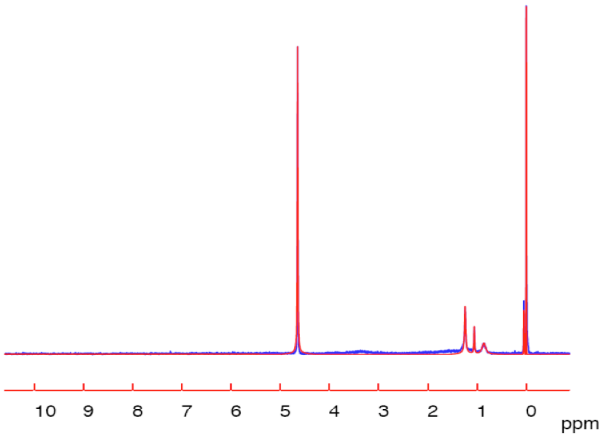

Number	δ [ppm]	I [-] (relative)	Correspondence in Table 1
1	4.65	1.00	row 4
2	1.24	0.54	water
3	1.05	0.15	Water
4	0.86	0.25	Water
5	0.05	0.17	TMS
6	0.00	0.86	TMS

D1. H_2 dissolved in the bulk solvent (CCl_4) in the presence of the porous solid (γ-alumina) + H_2 dissolved in the solvent (CCl_4) confined in the solid pores when the solid is soaked in bulk solvent (P = 110 kPa, T = 298 K, bulk solvent)

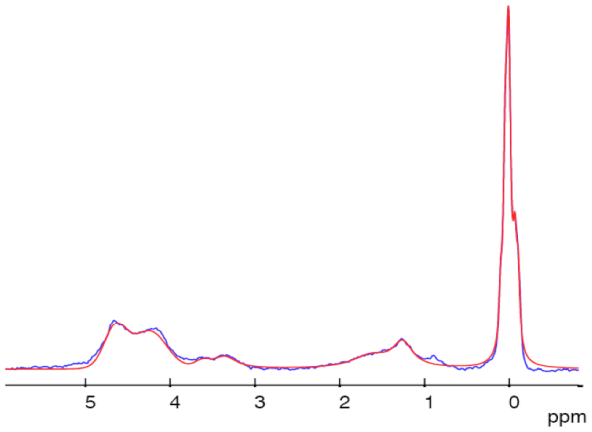

Number	δ [ppm]	Width [Hz]	I [-] (relative)	Correspondence in Table 1
1	4.67	91	1.00	row 5
2	4.49	72	0.24	row 5
3	4.20	100	0.84	row 6
4	3.37	99	0.21	Water
5	1.41	181	0.59	Water
6	1.25	56	0.13	Water
7	-0.01	99	1.21	TMS
8	0.00	46	2.19	TMS

D2. H_2 dissolved in the bulk solvent (CS_2) in the presence of the porous solid (γ-alumina) + H_2 dissolved in the solvent (CS_2) confined in the solid pores when the solid is soaked in bulk solvent (P = 110 kPa, T = 298 K, bulk solvent)

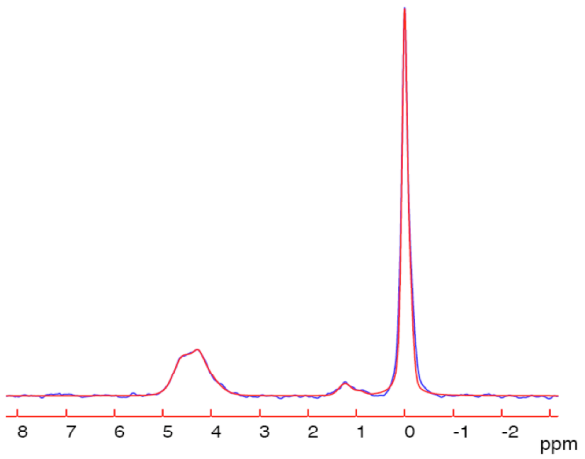

Number	δ [ppm]	Width [Hz]	I [-] (relative)	Correspondence in Table 1
1	4.62	112	1.00	row 5
2	4.21	136	1.58	row 6
3	-0.04	77	3.41	TMS
4	0.01	31	2.19	TMS

E2. H_2 in contact with the wet porous solid (γ-alumina + CS_2) + H_2 dissolved in the solvent confined in the solid pores when the gas/liquid interface is in the pore (P = 1.1 bar, T = 298 K, solvent loading = 69%)

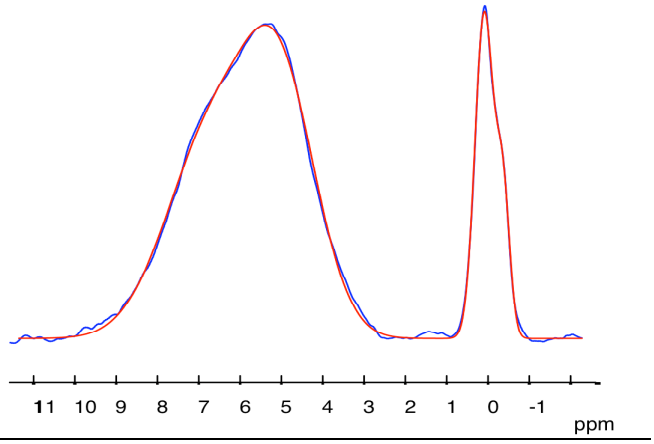

Number	δ [ppm]	Width [Hz]	I [-] (relative)	Correspondence in Table 1
1	6.50	689	1.00	row 3
2	4.92	455	0.55	row 7
3	0.10	137	0.27	TMS
4	-0.36	92	0.07	TMS

E1. H_2 in contact with the wet porous solid (γ-alumina + CCl_4) + H_2 dissolved in the solvent confined in the solid pores when the gas/liquid interface is in the pore (P = 110 kPa, T = 298 K, solvent loading = 34%)

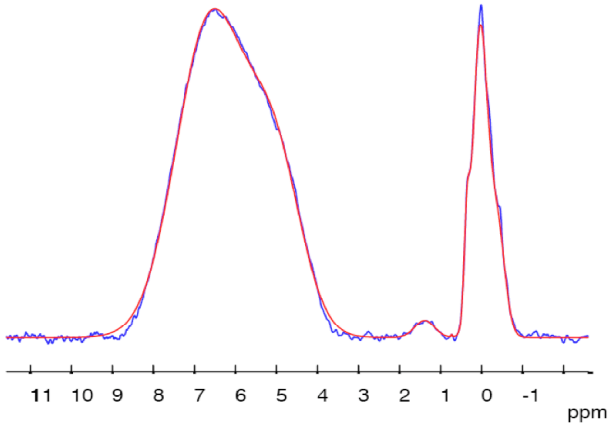

Number	δ [ppm]	Width [Hz]	I [-] (relative)	Correspondence in Table 1
1	6.66	575	1.00	row 3
2	5.13	479	0.48	row 7
3	1.43	239	0.02	water
4	0.33	67	0.05	TMS
5	-0.29	144	0.12	TMS
6	0.04	98	0.16	TMS

SI-d Calculation of the contribution of adsorbed CCl_4 layers on evacuated pores to porous volume and specific surface as a function of solvent loading

Calculation procedure: The contribution of adsorbed CCl_4 layers on both the specific surface and porous volume for a particular solvent loading, *f*, was computed from the BDB pore size distribution of γ-alumina and silica obtained from N_2 desorption at 77 K. In the calculations, capillary condensation of CCl_4 was assumed to occur from larger to smaller pores according to the Kelvin equation. CCl_4 adsorption was assumed to only take place in open pores by formation of a monolayer following the expression of Hakunan and Naono[26].

Notation: open and closed cycles refer to the porous volume of the probe solid occupied, respectively, by condensed and adsorbed CCl_4, while open and closed squares refer to the specific surface of the solid surrounded by condensed and adsorbed CCl_4, respectively. Contribution of adsorbed layer on porous volume and surface area <15% on right-hand side of dashed black line.

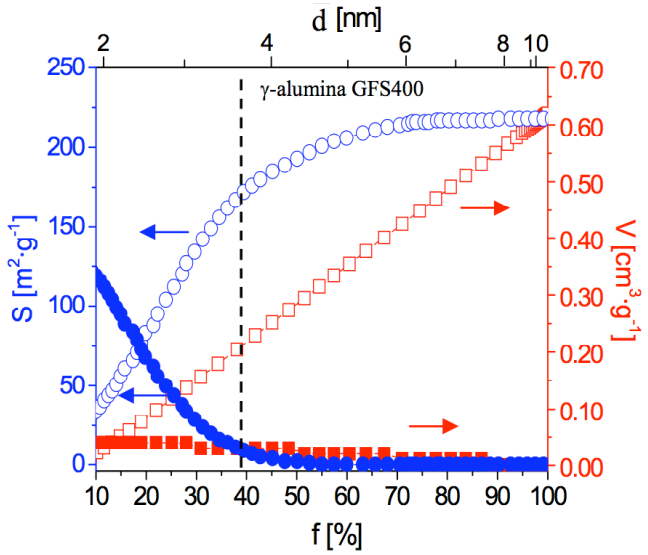

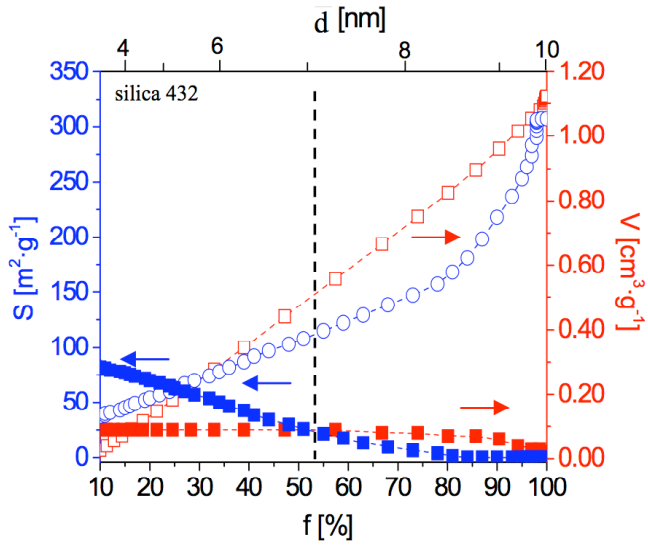

SI-e: Calculation of the contribution of solubility in nano-confined CCl_4 vs. gas adsorption on α-alumina evacuated pores. Evolution of nano-dissolved gas with the interfacial gas-liquid surface

Calculation procedure: In order to eliminate any possible influence of gas adsorption on the solids, conservative calculation of the mount of gas that could be adsorbed on γ-alumina for the case of H_2, CH_4 and C_2H_6 was carried out. It was assumed that the target gas only adsorbs on the open surface of the solid free from CCl_4 and that the adsorption strength is free from synergy effects with CCl_4. Moreover, the available interfacial gas-liquid surface for a particular solvent loading, *f*, was computed from the BDB pore size distribution of γ-alumina assuming that the pore is slit-shaped and that the depth of the pore approaches the mean diameter.

Notation: open and closed cycles refer to total experimental gas loading and possible adsorbed loading on γ-alumina, respectively, while open squares correspond to the interfacial gas-liquid surface available for dissolution.

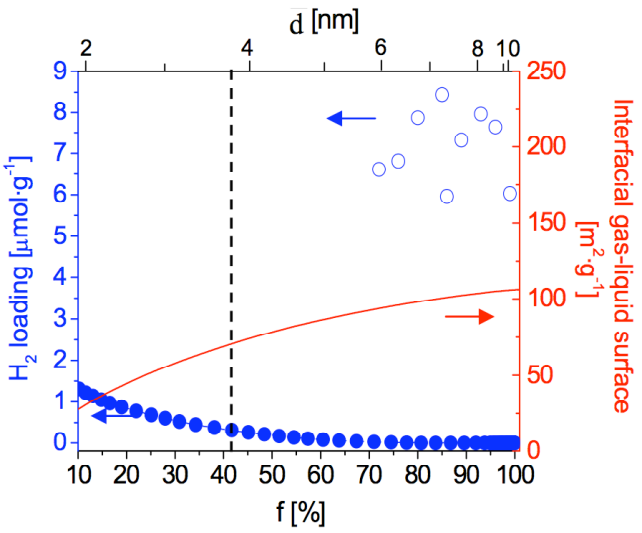

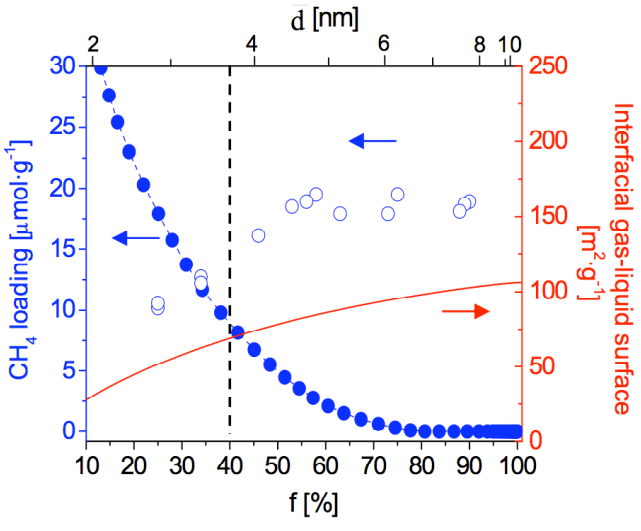

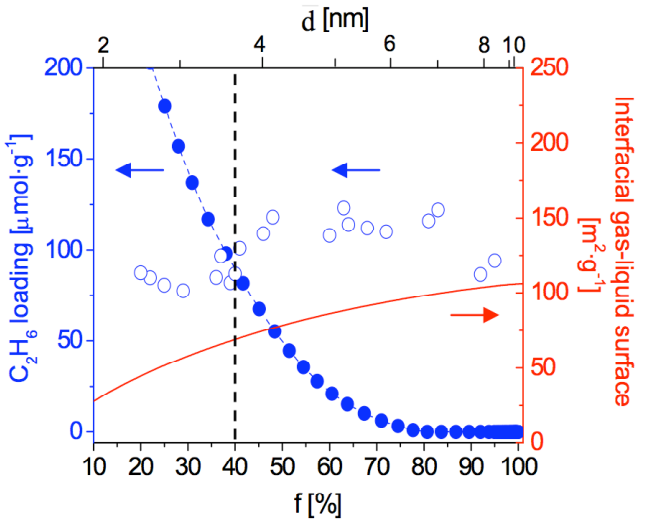

Note that in all cases, the amount of nano-dissolved gas is significantly larger than any possible gas adsorption on the γ-alumina surface for CCl_4 loadings above 40%. This loading corresponds to an adsorbed CCl_4 amount lower than 6% of its total loading. Moreover, the gas loading does not change much with CCl_4 loading in the range 60-100%, in agreement with the trend observed for the interfacial gas-liquid surface. Very similar results were obtained on silica support.

SI-f: Modeling. In the hypothesis of a gas-liquid interface confined in a slit-like mesopore, the overall gas solubility ℓ_g can be accounted by Eq. SI-1

$$\ell_g = \ell_g^{bulk} + \frac{v^i}{v}\left(\frac{\Gamma_g^{(1)}}{zC_G} - \ell_g^{bulk}\right) \qquad \text{(SI-1)}$$

where ℓgbulk is the bulk solubility, $\Gamma_{g(1)}$ is the excess surface gas concentration, and vi and v are, respectively, the interfacial and nano-liquid volumes. Assuming that the gas-liquid interface thickness, z, approaches the kinetic diameter of the adsorbed gas molecules, and that the mean pore size is close to its depth, Eq. SI-3 (Eq. 2 in the text) can be obtained for the overall gas solubility as a function of the nano-liquid mean size $\bar{d}$:

$$\ell_g = \ell_g^{bulk} + \frac{1}{\bar{d}}\left(\frac{\Gamma_g^{(1)}}{C_G} - z\ell_g^{bulk}\right) \qquad \text{(SI-2)}$$